Full Paper

Wiley Online Library

ELECTROANALYSIS

DOI: 10.1002/elan.202060581

Assessment of Corrosion Inhibition Performance and Adsorption Thermodynamics of Hydrogen Phosphate (HPO_4^{2-}) and Molybdate (MoO_4^{2-}) Oxyanions on Tin in Maleic Acid

Brahim Ait Addi,[a] Brahim El Ibrahimi,[a] Abdelaziz Ait Addi,[a] Abdul Shaban,*[b] El-Habib Ait Addi,[c] and Mohamed Hamdani[a]

Abstract: The influence of hydrogen phosphate (HPO_4^{2-}) and molybdate ions (MoO_4^{2-}) on the behavior of tin corrosion in 0.2 M maleic acid was compared using experimental and theoretical techniques. The experimental studies consisted of the electrochemical investigations (potentiodynamic polarization (PDP) and electrochemical impedance spectroscopy (EIS)), along with the surface analytical techniques (SEM and EDX). Additionally, the theoretical analysis (the chemical quantum computations at MP4/SDD level of theory in the aqueous phase), was conducted. The experimental outcomes illustrated that the inhibition efficiency (η%) increases with the concentration of the inhibitors, reaching 88 % and 81 % at 2×10^{-2} M concentration of MoO_4^{2-} and HPO_4^{2-}, respectively. The potentiodynamic polarization curves revealed that HPO_4^{2-} performance is a cathodic-type inhibitor, while MoO_4^{2-} shows a mixed-type behavior. The increase in temperature decreased the η% values of both inhibitors. Based on surface analysis and thermodynamic study, the presence of the two inhibitors formed protective films on the tin surface through a physisorption mechanism. The chemical quantum computations using the complete fourth-order Møller Plesset perturbation theory (MP4 with SDD basis) method results outlined the favorable affinity of the investigated inorganic inhibitors to interact with the tin surface, which interprets the well-observed inhibition efficiencies.

Keywords: Tin · corrosion · inhibition · molybdate · hydrogen phosphate · maleic acid

1 Introduction

Corrosion is a consequence of chemical or electrochemical reactions of the surrounding atmosphere with metals or their alloys. The damage magnitudes are significant in different fields, particularly in activities that require production disturbance, equipment replacement, serious accidents, and hazards of pollution are frequent events with considerable economic costs [1]. Generally, preventing corrosion is out of reach, but minimizing it is a possibility through several methods such as the application of corrosion inhibitors. Inhibitors function through different mechanisms, namely:

- Adsorption type: where the inhibitor is adsorbed on the metal surface developing a compacted protective thin film,
- Precipitation type: where the inhibitor formulates a precipitate on the metal surface or removes aggressive agents.

Inhibitors are named either cathodic, anodic or mixed inhibitors depending on their action on the cathode, the anode, or both sites, respectively [2–4].

Tin is extensively used as a protecting coating for steel in tin plate manufacture, namely tin cans. Steel (as a cathode) is the base metal of tin cans, while the inner subjected to food metal (tin) behaves as the anode.

The extent of tin cans corrosion is influenced by the conserved food content, whether acidic, basic, etc. Products containing acids cause the development of complexes which eventually leads to damaging the tin coating. The tin corrosion behavior and passivation in maleic, citric, tartaric, acetic, formic, carboxylic, and other acids have been analyzed in aqueous solutions [5].

[a] Dr. B. Ait Addi, Prof. B. El Ibrahimi, Prof. A. Ait Addi, Prof. M. Hamdani
Team of Physical Chemistry and Environment, Faculty of Science, Ibn Zohr University, Agadir, 80000, Morocco
[b] Dr. A. Shaban
Institute of Materials and Environmental Chemistry, Research Centre for Natural Sciences, Hungarian Academy of Sciences, Budapest, H-1117, Hungary
E-mail: shaban.abdul@ttk.mta.hu
[c] Prof. E.-H. Ait Addi
Biotechnology, Energy and Environment Group, High School of Technology, Ibn Zohr University, Agadir, 80150, Morocco

Inhibition of tin corrosion by the application of various organic and inorganic inhibitors is well documented. A wide-ranging variety of tin corrosion inhibitors such as different oils, epoxy phenolic lacquers, Sodium dodecyl-sulfate, amino acids, etc. were investigated and demonstrated effectiveness against tin corrosion [5–8].

Matched with other inhibitors, the important advantages of phosphates are economical and low toxicity [9,10]. Phosphates are wildly applied in the pretreatment of the rebar's or admixed into concrete [11–13]. Moreover, the advantageous effect of phosphate in chloride electrolyte has been attributed to their adsorption onto the passive layer, thus dislocating chloride ions and obstructing the initiation of localized corrosion of steel [14]. However, the electrochemical characteristics of the phosphate inhibitor are rather arguable where some researchers consider phosphates as anodic inhibitors that require oxygen to be effective, while other investigators classified them as cathodic inhibitors or as mixed-type inhibitors [12,15].

Several investigations reported the low toxicity and eco-friendly suitability of molybdate anions (MoO_4^{2-}), as tin corrosion inhibitors in different media [16,17]. In a previously published contribution, we demonstrated that molybdate anions hinder the pitting corrosion of tinplate in a synthetic media analogous to industrial water comprising chloride, sulfate, and hydrogen carbonate ions; the pitting phenomenon decelerated and simultaneously accelerate the uniform corrosion by involving the untinned process [18].

In this contribution, the inhibition efficiencies of MoO_4^{-2} and HPO_4^{2-} on the tin corrosion in 0.2 M maleic acid solution is examined by the electrochemical methods (potentiodynamic polarization (PDP), electrochemical impedance spectroscopy (EIS)), the surface analytical methods (the scanning electron spectroscopy (SEM) and the energy dispersive X-ray (EDX)). Besides, the effect of temperature alteration on the effectiveness of these inorganic compounds in the range of 25–60 °C is evaluated.

Chemical quantum computations using the complete fourth-order Møller Plesset perturbation theory (MP4 with SDD basis) method is performed to situate more emphasis on the MoO_4^{-2} and HPO_4^{2-} affinity to interact with the tin surface, which can interpret the excellent inhibition efficiencies.

2 Materials and Experimental Methods

2.1 Solutions and Chemicals

Tin corrosion inhibition investigations were performed in 0.2 M maleic acid solution in the absence and presence of molybdate (MoO_4^{2-}) and hydrogen phosphate (HPO_4^{2-}) oxyanions. The electrolyte solutions were prepared by dissolving analytical grade chemicals (p.a. Merck) in bi-distilled water. The tests were carried in a de-aerated solution (N_2 bubbling) at a pH = 1.8, and a temperature of 25 °C. All experiments were repeated in triplicates for reproducibility purposes.

2.2 Electrochemical Measurements

PDP and EIS experimentations were done in a classical 3-electrode cylindrical glass cell. The working electrode (WE) was made of a tin rod (Aldrich 99.99 %) axially embedded in "Araldite" holders (area = 0.785 cm^2). A saturated calomel electrode (SCE) and a Pt sheet were the reference and auxiliary electrodes, respectively.

Before each test, the WE surface was polished with different emery paper grades (down to 1200 grits), degreased using acetone, and quickly rinsed with bi-distilled water.

The electrochemical study was performed applying a potentiostat-galvanostat apparatus (PGZ 100), controlled by the Volta-Master software. PDP plots were obtained at a 60 mV/min potential scan rate. Before each electrochemical measurement, the WE was sustained at the open circuit potential (OCP) for 0.5 hr. of immersion time. All measured potentials are versus the SCE.

2.3 Surface Analysis Experiments

Tin pre-cleaned specimens were immersed in 0.2 M maleic acid solutions without and with the addition of inhibitors for 24 hrs. The specimens were washed with bi-distilled water and dried. The surface analysis was conducted using the SEM and EDX apparatus.

2.4 Quantum Chemical Computational

The initial molecular structure of considered inorganic inhibitor species and the calculation method is arranged using Gauss-View 5 software. The structural optimization and the calculation of relevant electronic structure parameters were performed using the MP4 method with an SDD basis set [19] as employed in Gaussian-9 software [20]. The solvation effect on inhibitor species was considered using the conductor-like polarizable continuum model through setting water as the solvent [21]. The full optimization practices show no presence of imaginary frequencies which was verified by analyzing the vibrational frequencies [22].

The energy of frontier molecular orbitals (E_{HOMO} and E_{LUMO}), energy gap (ΔE), global chemical hardness (η), expected a fractional number of electrons transferred (ΔN), total dipole moment (μ), and total negative charges (TNC) based on the natural population analysis (NPA), are among the available electronic structure parameters that describe the reactivity of inhibitors [23,24].

Since both tested inorganic inhibitors (MoO_4^{2-} and HPO_4^{2-}) are studied in an acidic environment (maleic acid), therefore both oxyanion compounds can undertake protonation or further protonation process at oxygen atoms. Accordingly, the study of additional protonated forms ($HMoO_4^-$ and $H_2PO_4^-$) of these species is essential

to get a comprehensive idea of the observed inhibition behaviors.

3 Results and Discussion

3.1 Potentiodynamic Polarization Curves

Figure 1 illustrates the cathodic and anodic polarization curves for the tin electrode in 0.2 M maleic acid at 25 °C, without and with the addition of 0.001, 0.01, and 0.02 M concentrations of HPO_4^{2-} and MoO_4^{2-}. The significant electrochemical parameters extrapolated from Figure 1 are summarized in Table 1.

It is observed that the tin behavior in the inhibitor-containing 0.2 M maleic acid is influenced by the oxyanion concentrations. The anodic region showed a decrease of the anodic current density due to the addition of both inhibitors, with a predominance of MoO_4^{2-}. This outcome can be accredited to the inhibitor species adsorption onto the surface electrode and then the formation of a protective film hindering admittance of aggressive species into the tin surface.

Table 1 displays that the corrosion current density drop with the increase of inhibitor concentration. Therefore, the addition of inhibitors to the corrosive solution leads to a regression of tin metal dissolution. It was reported that the E_{corr} displacement value of 85 mV between the blank and inhibited solution is the base for categorizing an inhibitor as either cathodic, anodic, or mixed-type inhibitor [25]. The obtained results disclosed that HPO_4^{2-} and MoO_4^{2-} demonstrated a cathodic and a mixed behavior type of inhibition, respectfully.

To quantitatively calculate the prevention ability of the tested oxyanions, the inhibition efficiency (η %) is evaluated using the next equation:

$$\eta\% = \frac{(I_{corr} - I_{corr-inh})}{I_{corr}} x100 \quad (1)$$

where $I_{corr-inh}$ and I_{corr} are the current densities with and without the addition of the inhibitor, respectively. The $I_{corr-inh}$ and I_{corr} values are extrapolated from the cathodic Tafel lines to the E_{corr}.

The effect of various concentrations of the tested inhibitors on the inhibition efficiencies is illustrated graphically in Figure 2. As shown in Figure 2, the inhibitory efficiency improved with increasing the C_{inh} of inhibitor oxyanions. This behavior is explained by the adsorption mechanism of inhibitors on the tin surface; in this regard, the adsorption process increased with enhancing the C_{inh} and hindered attack on the tin electrode by corrosive agents. The highest reached values of η were 81 and 88 % for HPO_4^{2-} and MoO_4^{2-}, respectively. This outcome designates that the tested inhibitors can obstruct the tin dissolution and surface destruction with different degrees where MoO_4^{2-} was superior. Additionally, the MoO_4^{2-} inhibition mechanism is generally associated with its adsorption on the tin surface initiating a decline of the metal surface with an aggressive solution besides hinder-

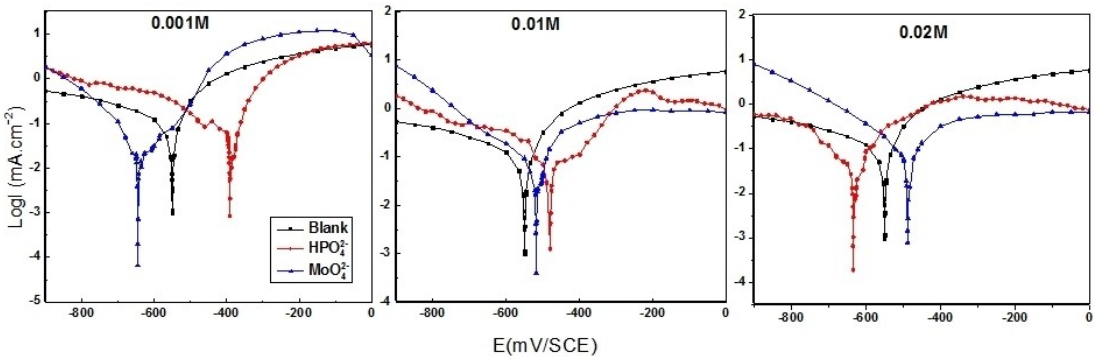

Fig. 1. Polarization curves for the tin electrode in 0.2 M maleic acid without and with the addition of different concentrations of HPO_4^{2-} and MoO_4^{2-} at 25 °C.

Table 1. Polarization parameters for tin corrosion in 0.2 M maleic acid in the absence and presence of hydrogen phosphate and molybdate anions at 25°C.

	C (M)	E_{corr} (mV_{SCE})	I_{corr} ($\mu A/cm^2$)	η (%)
Blank	0.2	−558	160	–
HPO_4^{2-}	0.001	−358	110	31.2
	0.01	−480	65	59.3
	0.02	−637	30	81.2
MoO_4^{2-}	0.001	−512	91	43.1
	0.01	−512	44	72.5
	0.02	−493	18	88.7

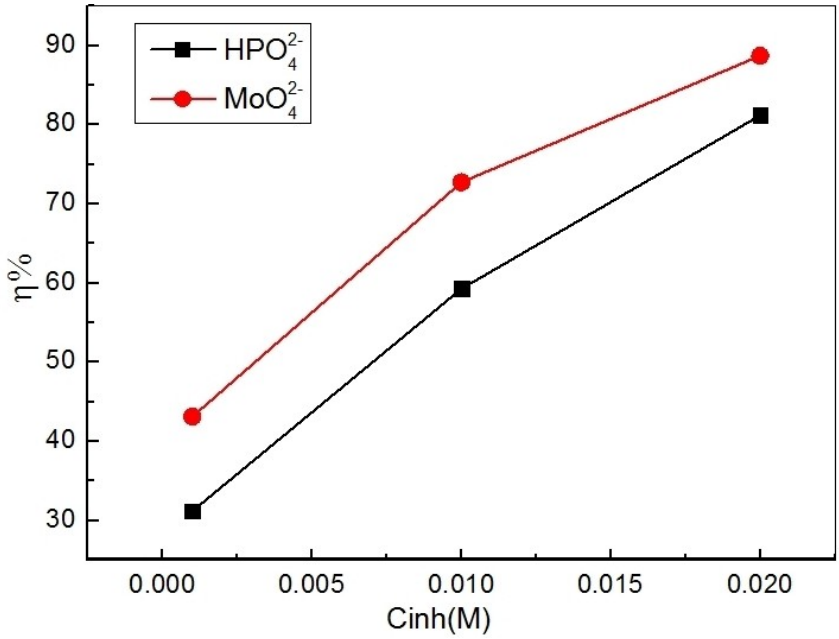

Fig. 2. Effect of inhibitor concentration of HPO_4^{2-} and MoO_4^{-2} on the inhibition efficiency at 25 °C.

ing active sites and therefore decreasing the metal dissolution reaction through the development of the coating film.

During the corrosion process, which is an electrochemical reaction, at the tin metal surface, there are two sites, namely: an anodic site corresponding to the oxidation process, called anodic reaction ($Sn \rightarrow Sn^{x+} + xe^-$) and a cathodic site related to reduction process, called cathodic reaction ($2H^+ + 2e^- \rightarrow H_2\uparrow$) in acidic media, as in this present case. Following the displacement of E_{corr} in the presence of the inhibitors as compared to the blank solution, the inhibitor can be classified into anodic (block the sites at the surface in which the oxidation of metal, Sn, is occurred), cathodic (block the sites at the surface in which the reduction of H^+ ions occur) or mixed-type inhibitor (block in the same time both sites).

As shown in Table 1, the largest displacements exhibited by HPO_4^{2-} and MoO_4^{2-} are 79 and 12 mV, respectively. E_{corr} shifted to a negative direction; although there was not a specific relation between E_{corr} and inhibitors C_{inh}. The negative shift in the case of HPO_4^{2-} indicates the inhibition of the acid corrosion of tin with predominantly control of the cathodic reaction. In the case of MoO_4^{2-}, from the obtained values, a mixed-type of inhibitor behavior is confirmed. This also indicates that the inhibitor merely blocks the reaction sites of the tin surface and changes the mechanism of metal dissolution (anodic) and/or hydrogen evolution (cathodic) reaction.

The action of those inhibitors on tin corrosion in maleic acid (org) is the formation of protective layers on the metal surface, which consist of Sn(org)ads. The formed films will disband at higher anodic potentials (more positive). As a result of the oxidation of tin, an oxide passive layer is formed. Adding the HPO_4^{2-} and MoO_4^{2-} ions to the electrolyte solution following the disappearance of the layer of Sn oxide, the protective layer was formed as follow:

$$Sn + HPO_4^{2-} \rightarrow SnHP\ O_4^{2+} + 2\ e^- \quad (2)$$

$$Sn + MoO_4^{2-} \rightarrow SnMoO_4^{2+} + 2\ e^- \quad (3)$$

$SnHPO_4$ and $SnMoO_4$ are formed by the interaction of the inhibitors with the surface of the tin electrode. The effectiveness of the protective layer hangs on the orientation of molybdate ions, relative to the tin surface. The donor centers are possibly the inhibitor.

On the one hand, the adsorption of oxysalt anions such as HPO_4^{2-} and MoO_4^{2-} on a passive film surface could modify the passive film from an anion-selective structure to a cation-selective structure, which could prevent the passive film from adsorption and attack by maleic acid solution. Since HPO_4^{2-} and MoO_4^{2-} are anions, the passive film with more Sn^{2+} would favor the adsorption of HPO_4^{2-} and MoO_4^{2-}.

3.2 Electrochemical Impedance Spectroscopy Plots

To obtain additional evidence on the inhibition procedure to support the PDP obtained results, EIS measurements, a powerful *ac*-technique to study the corrosion mechanism, were performed on the tin electrode in 0.2 M maleic acid. Nyquist plots for tin in 0.2 M maleic acid solution in the absence and presence of inhibitors, at different C_{inh} of HPO_4^{2-} and MoO_4^{-2} are shown in Figures 3 and 4, respectively.

At first, the Nyquist plots achieved in the blank solution exhibited two distinct peaks or relaxation-times.

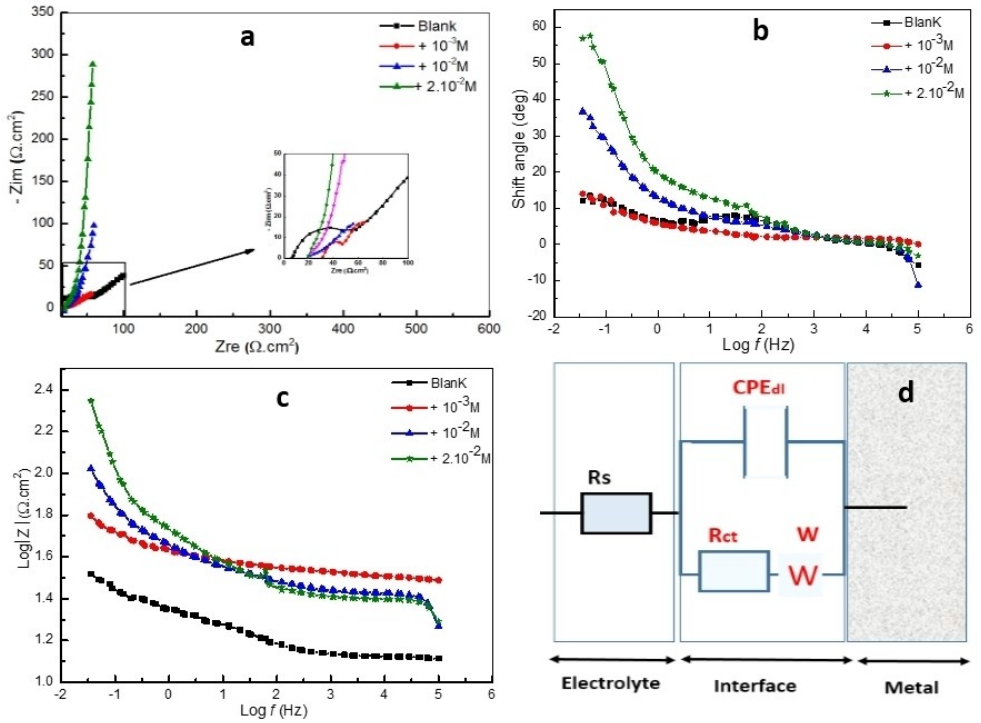

Fig. 3. EIS data of tin in 0.2 M maleic acid solution in the presence and absence of HPO_4^{2-} at various concentrations at 25 °C. (a) Nyquist plot; (b) Bode phase plot; (c) Bode magnitude plot; (d) Used equivalent electrical circuit.

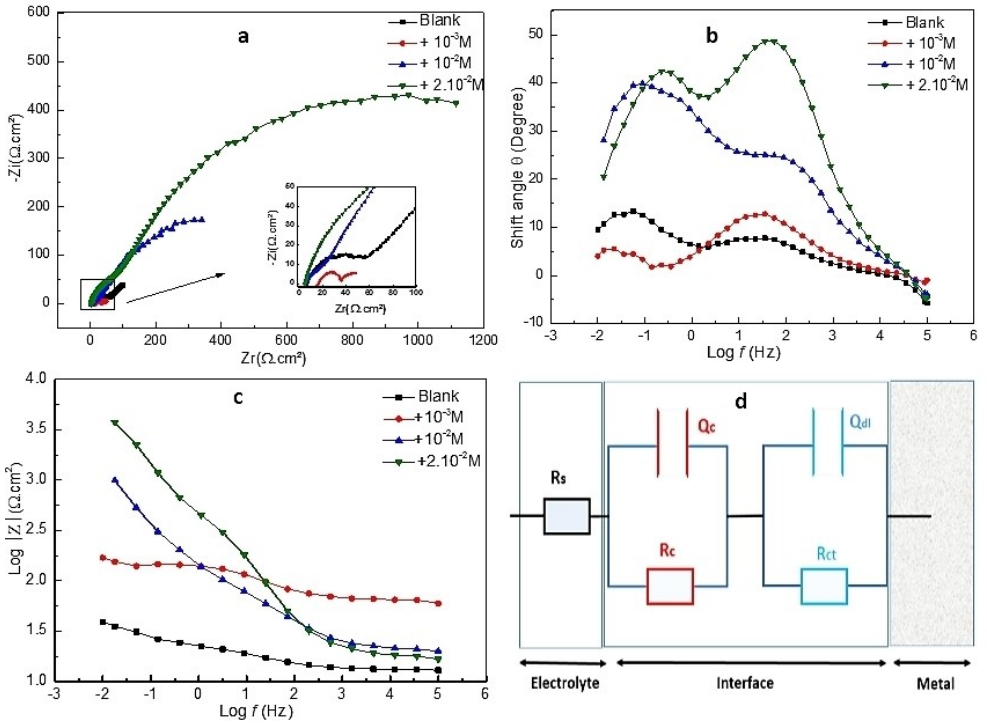

Fig. 4. EIS data of tin in 0.2 M maleic acid solution in the presence and absence of MoO_4^{2-} at various concentrations at 25 °C. (a) Nyquist plot; (b) Bode phase plot; (c) Bode magnitude plot; (d) Used equivalent electrical circuit.

The peak at the high frequencies (HF) region is accredited to a semicircle illustrating a capacitive loop,

while the peak at the low frequencies region (LF) shows a linear region, representative of the existence of a Warburg-diffusion type.

Furthermore, the addition of the tested inhibitors imperfect and modified the Nyquist plots semicircles, which is caused by the frequency dispersal related to the inhomogeneity of the tin electrode surface (Figures 3a–4a) [26].

On the other hand, a comparison of concentration-effect reveals that in the addition of HPO_4^{2-}, the Nyquist impedance diagram (Figure 3a) produced two distinct regions. At the HF region, a semicircle characterizing a capacitive loop is characterized by a charge transfer resistance (R_{tc}) and a double layer capacitor (C_{dl}). While in the LF region, the linear plateau is associated with a diffusional phenomenon in the liquid phase [27]. However, in the presence of MoO_4^{2-}, the Nyquist diagram (Figure 4a) showed two capacitive loops whose size increased with increasing the C_{inh} demonstrating the inhibitory effect of molybdate ions and its dependency on the C_{inh}. The HF peak characterizes the charge transfer phenomenon while the LF one defines the oxide film formed on the tin electrode surface.

Figures 3d and 4d, display the equivalent circuits simulating the tin electrochemical interface in 0.2 M maleic acid with and without inhibitor, obtained using the Zsimp-Win (V. 3.10) software, to calculate the parameters of the used elements. In Figure 3d, R_s signifies the solution resistance, R_{ct} represents charge transfer resistance, CPE is the constant phase element, and *W* denotes Warburg's diffusion impedance element. In the case of MoO_4^{2-}, the representative equivalent circuit consists of Q_c and R_c that correspond to the formed film on the tin surface in the HF range and of Q_{dl} and R_{tc} related to the charge transfer reaction in the LF range, as shown in Figure 4d. Remembering that the phase constant element denotes the relaxation times distribution for microscopic inhomogeneity existing at the metal/electrolyte interface [28].

Figure 5 shows that R_{ct} and I_{corr} values have the opposite trend (R_{ct} increases and I_{corr} decreases) due to the formation of a protective film as a result of the HPO_4^{2-} and MoO_4^{2-} ions adsorption on the tin surface. The obtained EIS is in good agreement with the PDP studies. Alternatively, the inhibition efficiency (η %) is calculated using Eq. (4) and demonstrated in Figure 6:

$$\eta\ \% = \frac{R_{ct-in} - R_{ct}}{R_{ct-in}} \times 100 \quad (4)$$

where $R_{ct\text{-}in}$ and R_{ct} are the value of charge transfer resistance of tin with and without the addition of inhibitor, respectively. As shown in Figure 6, the inhibition efficiency (η%) increases as a result of increasing the concentration of both oxyanions, which suggests that the effectiveness of the inhibitors is due to their adsorption on the tin surface thus hindering the tin dissolution rate.

3.3 Adsorption Parameters from Adsorption Isotherms

It is well acknowledged that the establishment of isotherms provides significant data about the metal/inhibitor interface. Both the Langmuir (Eq. 5) and Temkin (Eq. 6) isotherms are evaluated on the outputs of the applied electrochemical methods (PDP and EIS).

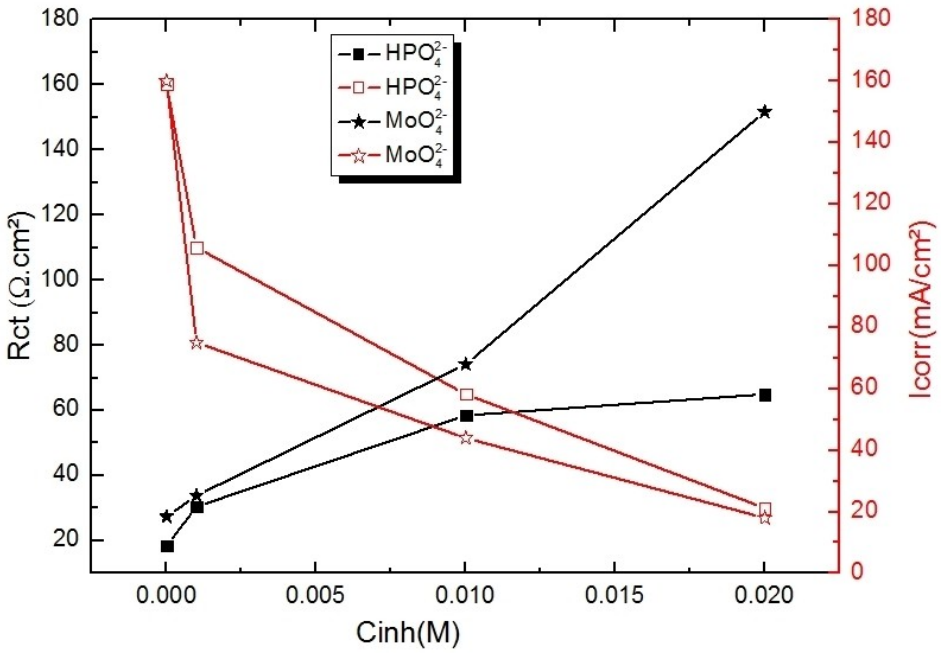

Fig. 5. Relationship between charge transfer resistance (R_{ct}) and corrosion current density (I_{corr}) as a function of concentrations of C_{inh}.

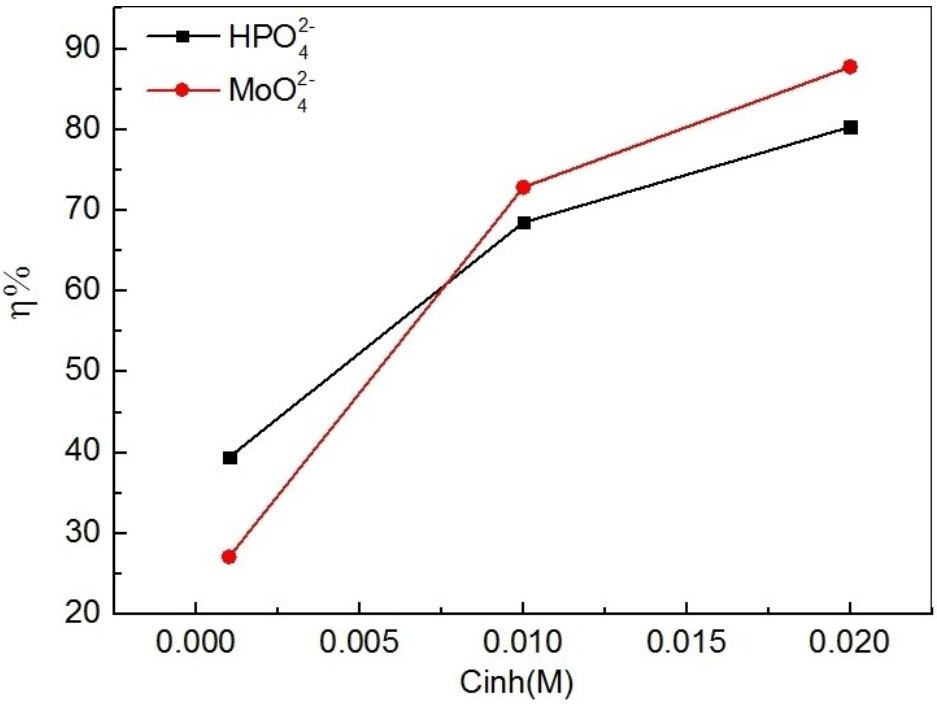

Fig. 6. EIS results of the dependence of inhibition efficiency on the inhibitor concentration at 25 °C.

Accordingly, for those isotherms, θ is associated with C_{inh} employing the following relationships:

$$\frac{C_{inh}}{\theta} = C_{inh} + \frac{1}{K_{ads}} \quad (5)$$

$$\exp(-2a\theta) = K_{ads} \times C_{inh} \quad (6)$$

where K_{ads} is the constant of the adsorption reaction and *"a"* is the lateral interaction labeling the molecular interactions in the adsorption layer and the surface heterogeneity.

Figure 7 represents the adsorption isotherms fitting of the EIS and PDP data acquired by measurements of the tin electrode in 0.2 M maleic acid with the addition of various concentrations of HPO_4^{2-} and MoO_4^{2-} at 25 °C. As shown in Figure 7, the plotting of Cinh/θ vs. C_{inh} produced a linear curve (straight line). This result indicates that the adsorption of HPO_4^{2-} and MoO_4^{2-} ions on the tin-surface/solution interface and obeyed the Langmuir adsorption isotherm, with a correlation coefficient ($R^2 > 0.9$) closer to 1 for both ions, endorsing the validity of the chosen model.

The values of the linear regression coefficient (R^2), slopes, and adsorption coefficients of the inhibitors are shown in Figure 7 as well and tabulated in Table 2. The increase in both inhibitors concentration caused an increase in the extent of adsorption and surface coverage due to the availability of a larger number of inhibitor molecules and consequently an increase in inhibition efficiency.

Table 2. Linear regression coefficient (R^2) and slopes of Langmuir plots, (PDP and EIS), for HPO_4^{2-} and MoO_4^{2-} adsorption on the tin in 0.2 M maleic acid at 25 °C.

Inhibitor		Slope	R^2
HPO_4^{2-}	PDP	1.1211	0.9302
	EIS	1.742	0.9885
MoO_4^{2-}	PDP	1.0605	***0.9766***
	EIS	1.0003	***0.9929***

Although the linearity of the Langmuir plots (Figure 7.a) may recommend that the adsorption of inhibitor obeys the Langmuir isotherm model, the considerable deviation of the slope from unity (1.1211 and 1.742 for HPO_4^{2-}) exposed that the model does not represent the HPO_4^{2-} adsorption. The case for MoO_4^{2-} (slopes = 1.0605 and 1.0003) are slightly varied from the value of 1, which suggests that it fits better the model.

One more point to ponder, for the derivation of the Langmuir isotherm equation, it was assumed that the adsorbed molecules don't interact with one another, which is not actually in the case of the HPO_4^{2-} and MoO_4^{2-} ions. Such adsorbed inhibitor ions interrelate by joint repulsion-attraction forces which can disturb the slope (Figure 7). The alteration of the slopes could also be related to the variations in adsorption heat with increasing the surface coverage due to the increase in C_{inh} [29,30].

In the case of HPO_4^{2-}, researchers have attributed the inhibition behavior to the development of a thin layer on the tin surface [1,3,29]. Additionally, the tin surface in contact with the aggressive solution grows to be electron-

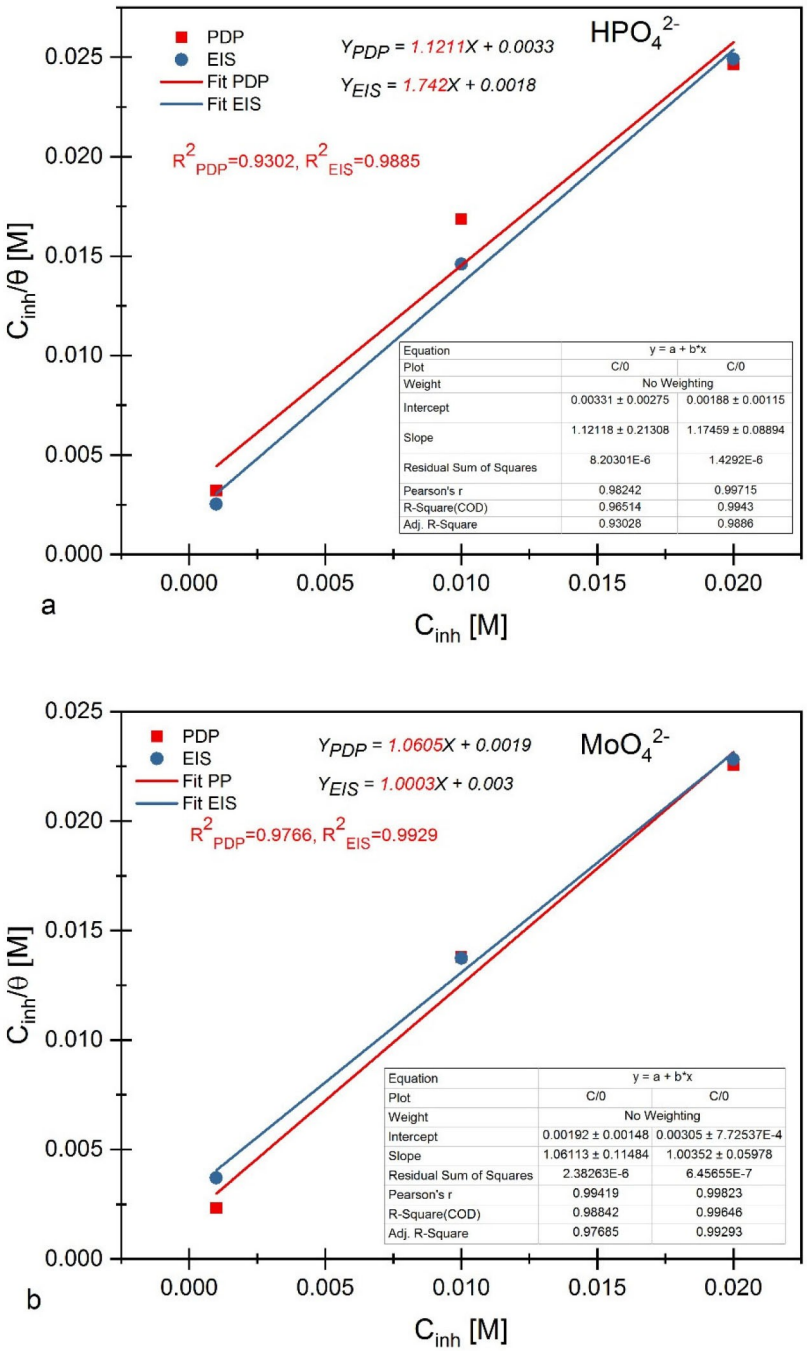

Fig. 7. Langmuir adsorption plots for tin in 0.2 M maleic acid-containing different C_{inh} of HPO_4^{2-} (a) and MoO_4^{2-} (b) at 25 °C.

deficient. This implies that positively charged and higher electron density centers in inhibitors anions adsorb on the tin metal surface forming a protective film. Whereas, in the case of MoO_4^{2-}, some investigators showed the adsorption of metal cations and oxides, on the anodic sites of the tin electrode surface, through the electrostatic attraction process [30].

The molybdate anions inhibition of tin corrosion can be accredited to the reduction process of the Mo^{6+} (as MoO_4^{2-}) to Mo^{4+} (as MoO_2) during the coating complex development [31]:

$$MoO_4^{-2} + 4H^+ + 2e^- \rightarrow MoO_2 + 2H_2O \quad (7)$$

As molybdate anions are reduced, more oxygen anions are produced which might inhibit the capacity of the aggressive anions to reach the metal/coating interface, probably by hindering the penetration to the protection film.

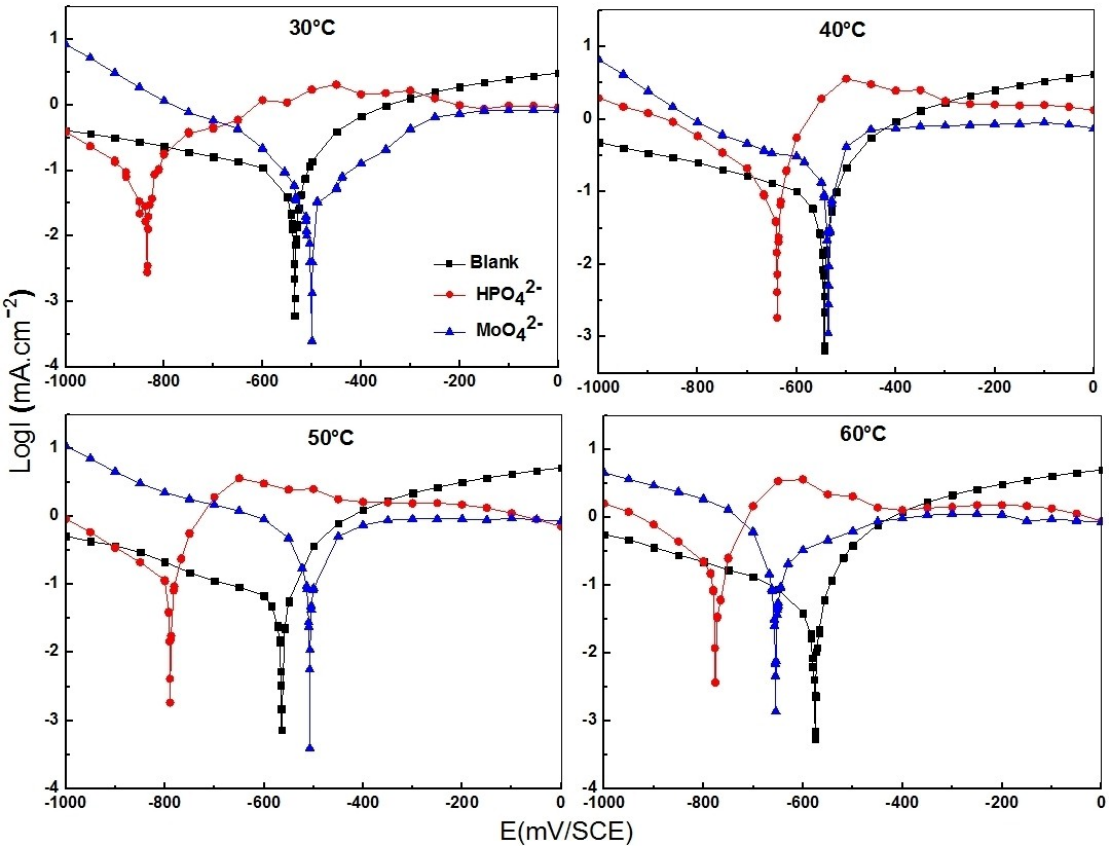

Fig. 8. PDP curves for tin in 0.2 M maleic acid in the absence and presence of 2×10^{-2} M HPO_4^{2-} and MoO_4^{2-} at different temperatures.

3.4 Influence of Temperature on the Inhibition Efficiency

Temperature is an important variable affecting the phenomenon of corrosion and its inhibition. The influence of temperature on the corrosion inhibition of tin in 0.2 M maleic acid at 2×10^{-2} M of HPO_4^{2-} and MoO_4^{2-} was investigated at 25, 30, 40, 50, and 60 °C. Figure 8 and Table 3 represent the obtained PDP curves and the corresponding interpolated electrochemical data, respectively.

As shown in Figure 8, increasing the test temperature caused a visible upsurge in both the anodic and cathodic current densities of the tin electrode in the presence of both HPO_4^{2-} and MoO_4^{2-}. Besides, in the anodic region the tin electrode surface passivation took place despite the temperature increase, but in a reverse trend as reported in the concentration-effect tests.

Table 3 shows that in both inhibited solutions the corrosion current density increased as the test temperature was increased. Also, the addition of 2×10^{-2} M HPO_4^{2-} shifted the corrosion potential (E_{corr}) towards more cathodic values (more negative), while in the case of MoO_4^{2-} the E_{corr} shift was lightly anodic (less negative). Previously, there was not a specific relationship between E_{corr} and inhibitor concentration.

The decrease of the inhibition efficiency when temperature increased from 25 to 60 °C is explained by a predominance of tin corrosion in maleic acid solution as compared to the adsorption of $HPO_4^{2-}$and MoO_4^{2-} active ions on the tin surface caused by the instability of the formed film. In this regard, the increase in temperature shifts the equilibrium in favor of the desorption process than the adsorption process, which demonstrates that the adsorption of the inhibitor molecule on the metal surface

Table 3. Temperature influence on the electrochemical parameters of the tin electrode in 0.2 M maleic acid with HPO_4^{2-} and MoO_4^{2-} at 25, 30, 40, 50, and 60 °C.

	T (°C)	E_{corr} (mV)	I_{corr} (μA/cm^2)	η %
Blank	25	−540	160	–
	30	−535	166	–
	40	−544	171	–
	50	−564	179	–
	60	−575	188	–
HPO_4^{2-}	25	−837	30	81.2
	30	−798	55	66.8
	40	−634	72	57.8
	50	−776	93	48.0
	60	−768	129	31.3
MoO_4^{2-}	25	−493	18	88.7
	30	−533	45	72.8
	40	−503	102	40.3
	50	−531	110	38.5
	60	−651	125	33.5

is a physisorption interaction. Furthermore, it is well known that the physisorption is due to weak van der Waal's forces, which disappear at elevated temperatures.

Figure 9 illustrates the reduced inhibition efficiency performance of the inhibitors owed to the desorption process of the anions from the tin surface at higher temperatures.

3.5 Activation and Thermodynamic Parameters

In order to obtain additional data about the tin corrosion and its inhibition mechanism, the calculations of the activation energy (E_a) employing the Arrhenius equation concerning the corrosion current density and the temperature, without and with the addition of the inhibitors, was accomplished by applying the following form [32]:

$$i_{corr} = K \times e^{-E_a/R\times T} \quad (8)$$

where i_{corr} is the current density ($A\,cm^{-2}$), K is the pre-exponential constant, E_a is the activation energy of the corrosion process ($kJ\,mol^{-1}$), R is the universal gas constant ($R = 8.31\,J\,mol^{-1}\,K^{-1}$), and T is the absolute temperature (K).

The dependence of Log (i_{corr}) on the inverse of the temperature (1/T) for the tin electrode in 0.2 M maleic acid without and with the addition of 2×10^{-2} M of HPO_4^{2-} and MoO_4^{2-}, is shown in Figure 10. The obtained plot in Figure 10, reveals that the relation *Log (i_{corr}) = f(1000/T)* follows linear behavior and follows the Arrhenius equation, both in the absence and in the presence of HPO_4^{2-} and MoO_4^{2-} inhibitors. The calculated values of the activation energy after the exploitation of these curves are $E_a = 3.21\,kJ\,mol^{-1}$ for the blank solution; $E_{a(inh)} = 26.69$ and $54.39\,kJ\,mol^{-1}$ in the presence of 2×10^{-2} M HPO_4^{2-} and MoO_4^{2-}, respectively.

A comparison of the obtained activation energies showed that the activation energy of both inhibitors are far greater than that for the blank solution ($E_{a(inh)} > E_a$), which further supports that both tested ions can shield the tin metal by adsorbing on the surface through electrostatic interactions. Nevertheless, the resultant type of temperature-sensitive bonding does not provide effective protection against tin corrosion as a result of the temperature increases [33]. It was designated that the activation energy increase leads to a corrosion rate reduction on the metallic surfaces [34]. Similarly, the inhibitor adsorption of the metal surface can hinder the metal dissolution rate by either decreasing the accessible dissolution sites, a.k.a. the geometric blocking effect, or by modifying the electrochemical reactions occurring at the metal/solution interface during the inhibition process [35].

Some investigations demonstrated similar behavior by investigating the mild steel corrosion inhibition by HPO_4^{2-} ions in NaCl solution of [10]. In an earlier contribution, it was shown that in a contradictory tendency, the addition of MoO_4^{2-} ions to a synthetic medium stimulates the dissolution of tinplate regardless of raising the temperature [18].

The free energy of the adsorption process ($\triangle G_{ads}$) can be estimated from the K_{ads} value:

$$\Delta G_{ads} = -RT\ln(K_{ads} \times 55.5) \quad (9)$$

where the constant 55.5 is the concentration of water, R is the universal gas constant and T is the absolute temperature.

As shown in Table 4, the negative values of standard free energy of adsorption designate spontaneous adsorption of inorganic ions on the tin electrode surface and also the strong interaction between inhibitor molecules and metal surface. The $\Delta G°_{ads}$ value of $-40\,kJ\,mol^{-1}$ is

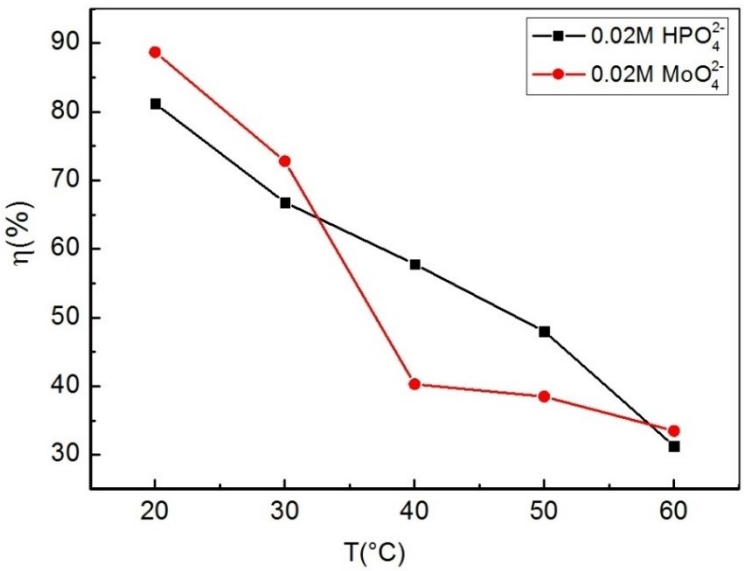

Fig. 9. Temperature effect on the inhibition efficiency of HPO_4^{2-} and MoO_4^{2-} against tin corrosion in 0.2 M maleic acid.

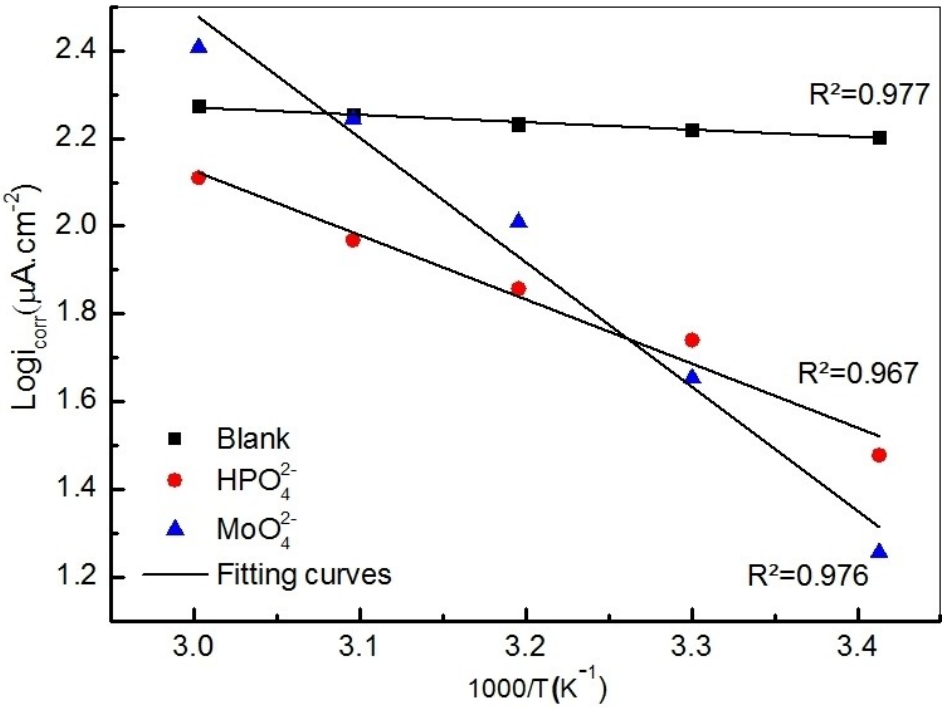

Fig. 10. Log (i_{corr}) = f (1000/T) plots of tin in 0.2 M maleic acid without and with 2×10^{-2} M of HPO_4^{2-} and MoO_4^{2-}.

Table 4. Thermodynamic parameters attained from the adsorption of HPO_4^{2-} and MoO_4^{2-} in 0.2 M maleic acid at 25 °C.

Inhibitor		K_{ads} (mol^{-1})	ΔG^{o}_{ads} ($kJ.mol^{-1}$)	R^2
HPO_4^{2-}	PP	0.0033	−23.70	0.930
	EIS	0.0018	−25.17	0.988
MoO_4^{2-}	PP	0.0019	−25.04	0.976
	EIS	0.0030	−23.93	0.992

considered the threshold value between chemical and physical adsorption processes [36]. Values up to −20 kJ mol^{-1} propose physisorption while values less than −40 kJ mol^{-1}, are representative of chemisorption [37–38]. Thus, for the present scheme, the ΔG°_{ads} values are in an intermediate-range which proposes comprehensive adsorption: a combination of both physical and chemical adsorptions dominated by physisorption.

3.6 Surface Analysis

3.6.1 Surface Characterization by Scanning Electron Microscopy

Figure 11 displays the SEM micrographs of a tin specimen immersed, for 24 hrs., in solutions with and without the addition of 2×10^{-2} M of $HPO_4^{2-}$and MoO_4^{2-}. Figure 11.a exposes the tin surface damage in the blank solution, as pits and cracks on the electrode surface are visible. Figure 11.b and 11.c show the intact tin surface with scarcer pits and cracks developed on the tin surface in the presence of $HPO_4^{2-}$and MoO_4^{2-}. The improved surface protection of the inhibited tin surfaces resulted because of the protective film formation by the two inhibitors over the tin surface, which isolated the surface active sites from the aggressive solution and thereby protecting it. It is worth mentioning that the tin surface protection obtained in the presence of MoO_4^{2-} was particularly more effective than HPO_4^{2-} (Figures 11.b, and 11.c), which supports the electrochemical results discussed beforehand.

3.6.2 Energy-dispersive X-ray Spectroscopy

EDX analysis is carried to recognize the adsorbed components on the tin specimen surface. Figure 12 illustrates the EDX spectrum of the tin surface in 0.2 M maleic acid in the absence (12.a) and presence of $2x10^{-2}$ M of HPO_4^{2-} (12.b), and MnO_4^{2-} (12.d) after 24 hrs. of immersion at 25 °C, with the composition (%) of elements present on the surface. It can be noted from the EDX analysis results that the tin elemental percentage on the uninhibited metallic specimen (Figure 12.a) is greater than that of the inhibited tin specimens in the presence of HPO_4^{2-} (Figure 12.b) and MnO_4^{2-} (Figure 12.c). Additionally, the order of the low intensity of EDX signal for atomic oxygen is in increasing order as follows: blank < blank + HPO_4^{2-} < blank + MoO_4^{2-}. Based on the EDX analyses, the strong ability of the HPO_4^{2-} and MoO_4^{2-} oxyanions adsorbed on the tin metal surface and thus developing a protecting layer, which shields the metal from the aggressive species and hinders the metal

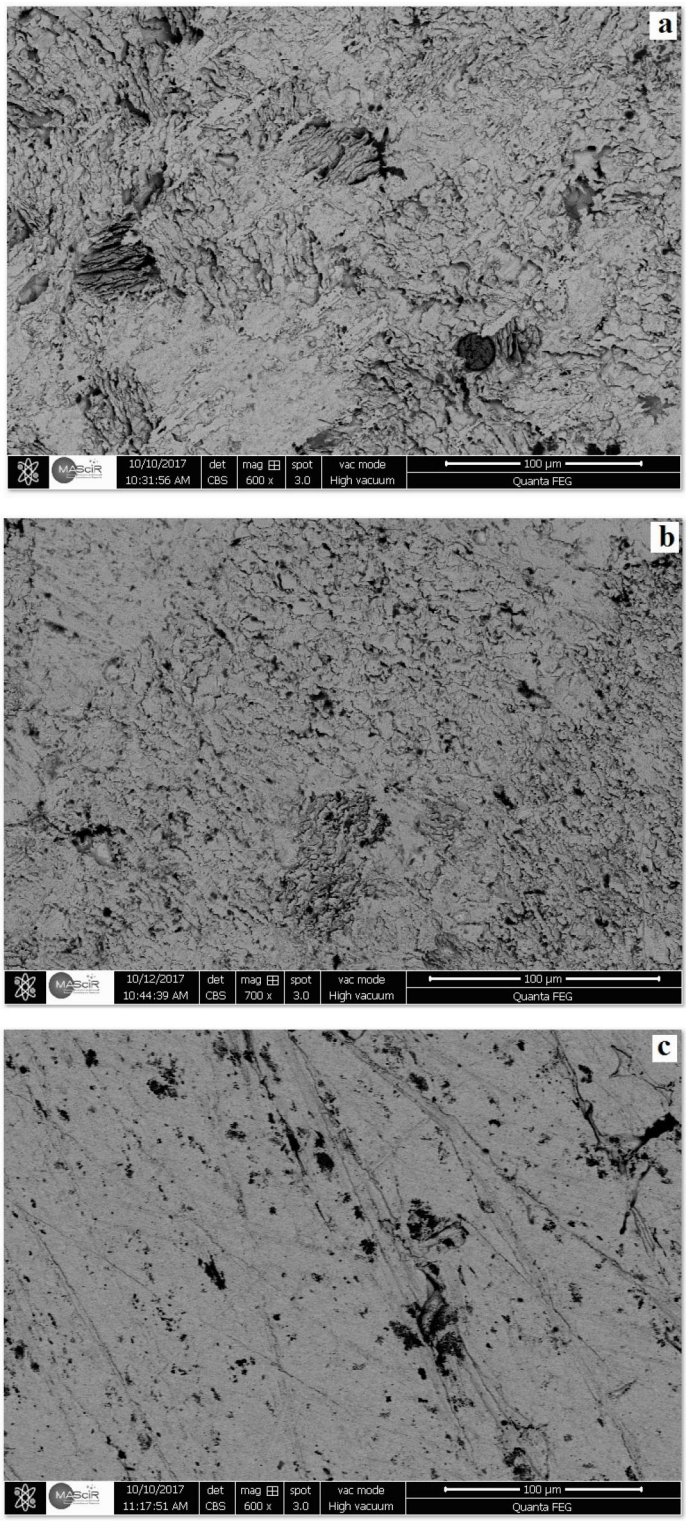

Fig. 11. SEM image of the tin surface in blank 0.2 M maleic acid (a), in the presence of $2x10^{-2}$ M HPO_4^{2-} (b), and MoO_4^{2-} (c), after 24 hrs. of immersion time.

dissolution process. These results confirm and support the preceding obtained results.

3.7 Quantum Chemical Study

Quantum chemical-based calculations were extensively applied procedures to examine the molecular and elec-

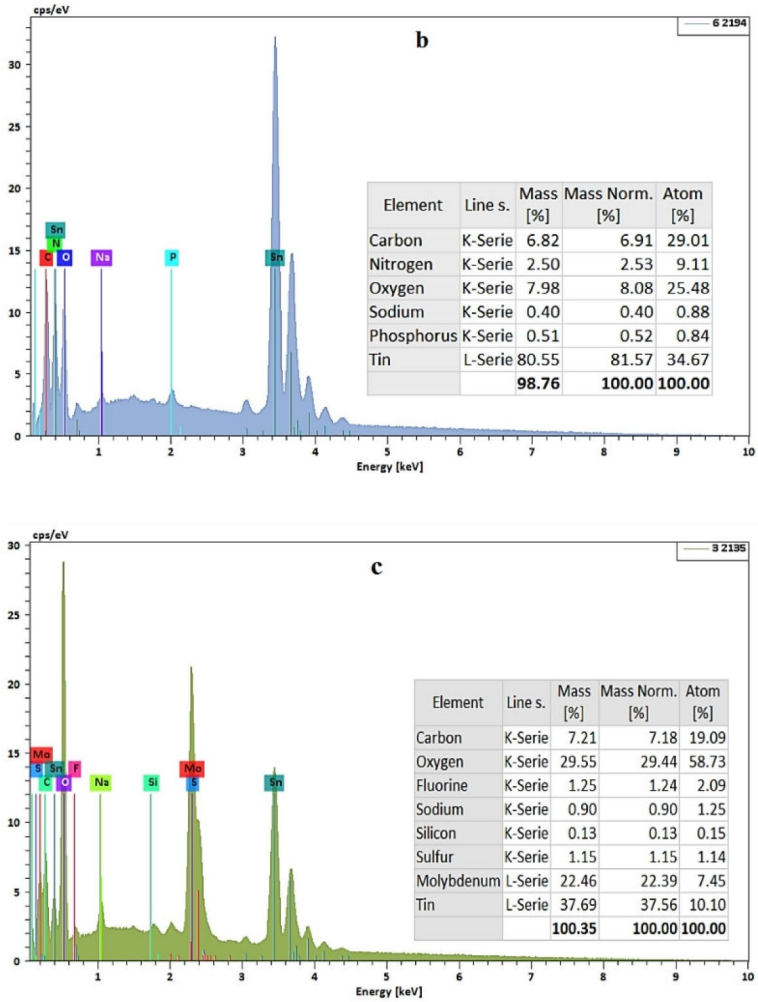

Fig. 12. EDX analysis of the tin surface in blank 0.2 M maleic acid (a), in the presence of $2x10^{-2}$ M HPO_4^{2-} (b), and MoO_4^{2-} (c), after 24 hrs. of immersion time.

tronic structures of numerous metallic corrosion inhibitors [39]. In this respect, calculations using the complete fourth-order Møller Plesset perturbation theory (MP4 with SDD basis) method in the aqueous phase were carried out on all considered inhibitor species. Given the optimized molecular structures of these species (Figure 13), some relevant electronic structure parameters were computed based on *.chk Gaussian files and listed in Table 5.

According to the Frontier Molecular Orbital (FMO) theory, the frontier molecular orbitals can be attended as indicators of reactivity. A molecule with a high E_{HOMO} and a low E_{LUMO}, which corresponding to a lower energy gap (ΔE), can display higher reactivity as compared to the molecule with an opposite trend [40].

In several investigations, the higher reactivity of the inhibitor molecule was correlated with the good inhibition ability [41]. The projection of this relationship on the tabulated values in Table 5 reveals that MoO_4^{2-} and $HMoO_4^-$ inhibitor species are more reactive than phosphate ones. This can explain, in part, the good

Table 5. Relevant electronic structure parameters of MoO_4^{2-}, $HMoO_4^-$, HPO_4^{2-} and $H_2PO_4^-$ species with MP4/SDD level under implicit solvation circumstance.

Species	E_{HOMO} (eV)	E_{LUMO} (eV)	ΔE (eV)	η (eV)	ΔN (e)	μ (D)	TNC (e)
MoO_4^{2-}	−10.218	0.782	11.000	5.500	−0.027	0.003	−3.896
$HMoO_4^-$	−11.343	0.529	11.872	5.936	−0.083	3.091	−3.644
HPO_4^{2-}	−9.975	6.309	16.284	8.142	0.159	4.979	−5.044
$H_2PO_4^-$	−11.498	4.818	16.316	8.158	0.066	7.557	−4.655

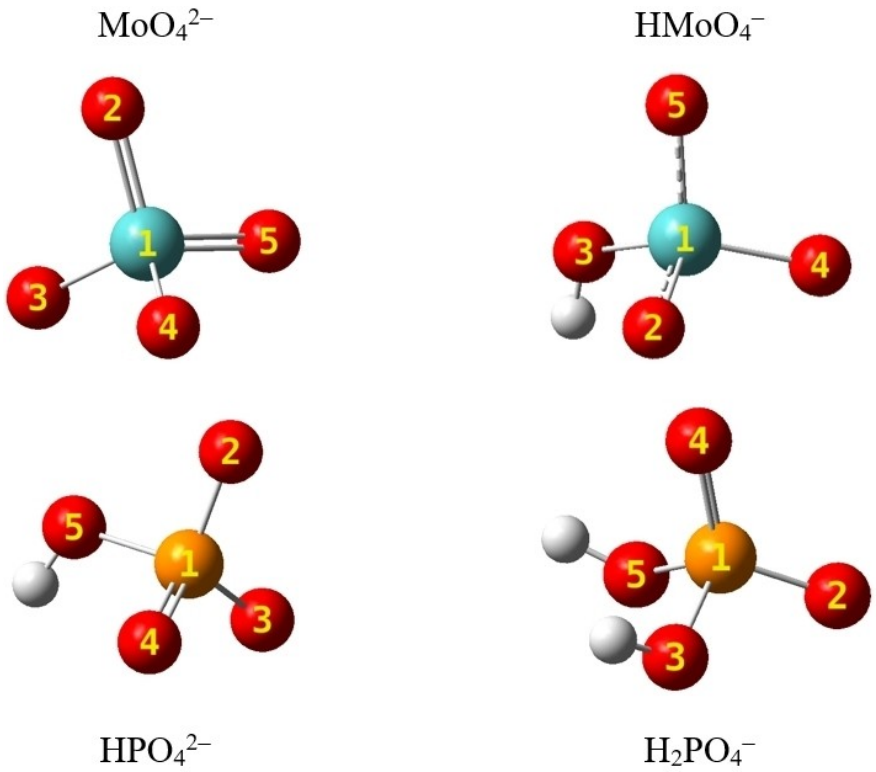

Fig. 13. Optimized molecular structure of MoO_4^{2-}, $HMoO_4^-$, HPO_4^{2-} and $H_2PO_4^-$ species at MP4/SDD level under implicit solvation condition (CPCM, water).

inhibition effectiveness achieved experimentally for MoO_4^{2-} oxyanions.

Furthermore, it is noted that that the protonation process of MoO_4^{2-} and HPO_4^{2-} follows a reduction of ΔE, which involves less reactivity of protonated species. A similar tendency was described elsewhere for several inhibitor compounds [42,43].

The global chemical hardness (η) signifies another indicator of reactivity which is largely used to investigate the inhibition behavior [44,45]. It was stated that a lower hardness value leads to less stability (i.e. more reactive) of a compound [46], which was associated with the higher inhibition capacity. Based on the obtained η values in Table 5, MoO_4^{2-} and $HMoO_4^-$ species exhibited higher reactivity in comparison to HPO_4^{2-} and $H_2PO_4^-$. Therefore, the molybdate inhibitor demonstrated improved corrosion inhibition capability than the phosphate inhibitor, in total agreement with the previously discussed experimental results.

As reported by some researchers, the interfacial inhibitor/metal surface electron flow can be implicitly estimated through the fractional number of electrons transferred (ΔN) parameter [47]. In this investigation, ΔN was calculated using the work function of the Sn (111) surface [48]. Given the obtained ΔN values (Table 5), both molybdate species, i.e. MoO_4^{2-} and $HMoO_4^-$, tend to accept electrons from the tin surface, which can proceed to the reduction of Mo (vi) (MoO_4^{2-} or $HMoO_4^-$) in Mo (iv). Whereas HPO_4^{2-} and $H_2PO_4^-$ oxyanions are anticipated to denote electrons to the metal surface [49].

Furthermore, the comparative analysis of these values emphasizes the stronger affinity of $HMoO_4^-$ and HPO_4^{2-} anions to exchange electrons with the tin surface than MoO_4^{2-} and $H_2PO_4^-$. Such an interfacial process results in the development of an adsorbed protecting layer onto the tin metal surface, which endorses the observed inhibition capability of these oxyanions.

The total dipole moment (μ) of an inhibitor can be exploited to estimate the electrostatic interactions at the inhibitor/tin interface [50]. Table 5 indicates that the higher μ values are established for the phosphate species. Such outcomes allow the anticipation that the electrostatic interaction nature of these agents with the tin surface. Alternatively, great μ values were found for the considered protonated species for both investigated inorganic inhibitors, particularly in the case of $H_2PO_4^-$. This highlights its affinity to interact electrostatically with the tin surface. Taking into consideration the observed inhibition efficiency (η %) and the calculated dipole moment, the decent (η %) of the molybdate inhibitor can be associated with its lower μ values, as previously reported [51].

Total negative charge (TNC) calculated from the natural population analysis (NPA), as shown in Table 6, is generally applied to analyze the inhibition process

Table 6. Atomic charges in different considered species constructed on the natural population analysis (numbering of atoms as in Figure 13).

Species	1	2	3	4	5
MoO_4^{2-}	1.897	−0.974	−0.974	−0.974	−0.974
$HMoO_4^-$	2.107	−0.864	−1.056	−0.865	−0.859
HPO_4^{2-}	2.531	−1.297	−1.301	−1.301	−1.145
$H_2PO_4^-$	2.568	−1.215	−1.109	−1.222	−1.109

[52,53]. In this perspective, the lower TNC value points out the increasing of the electrostatic interaction of the inhibitor with the positively-charged tin metallic surface in acidic media [54]. According to this correlation, it can be anticipated that phosphate species interact more electrostatically with the tin surface than molybdate species. This confirms the supposition previously drawn from the analysis of the total dipole moment.

4 Conclusions

The obtained results showed that HPO_4^{2-} and MoO_4^{2-} oxyanions hindered the tin corrosion in 0.2 M maleic acid solutions to significant degrees. The obtained η% values for HPO_4^{2-} and MoO_4^{2-} increased with increasing C_{inh}, however, decreased considerably with the increase of the solution temperature.

PDP revealed that HPO_4^{2-} and MoO_4^{2-} acted as a cathodic-type and mixed-type inhibitor, respectively. EIS measurements demonstrated that charge transfer resistance (R_{tc}) increased with increasing the C_{inh} of the two inhibitors which produced improved η% values. The obtained PDP and EIS results are in good agreement.

The adsorption of HPO_4^{2-} and MoO_4^{2-} obeyed the Langmuir adsorption isotherm, in which the formation of a protective film against acid attack was confirmed by SEM and EDX surface methods.

The chemical quantum calculations (MP4/SDD in water) defined the good affinity of investigated inorganic inhibitors to interact with the tin surface, which explains their good ability to inhibit tin corrosion. Furthermore, both considered molybdate species (i.e. MoO_4^{2-} and $HMoO_4^-$) desire to receive electrons from the tin surface, which can lead to the reduction of the Mo^{6+} to Mo^{4+}, therefore the establishment of a protective passive layer on the tin surface.

Acknowledgment

This contribution is part of a collaboration framework agreement between the Faculty of Science, Ibn Zohr University, Agadir, Morocco, and the Research Centre for Natural Sciences (TTK-AKI), Budapest, Hungary.

Data Availability Statement

The data that support the findings of this study are available from the corresponding author, [A. Shaban], upon reasonable request.

References

[1] S. B. Lyon. Corrosion of tin and its alloys. In *Shrier's Corrosion*, *4th ed., vol 3*; Elsevier B. V.: Amsterdam, The Netherland, **2010**, pp. 2068–2077.
[2] V. S. Sastri, *Corrosion Inhibitors, Principles and Applications*, Wiley, London, UK **1998**.
[3] F. A. Ansari, Y. S. Siddiqui, M. A. Quraishi, *Int. J. Corros. Scale Inhib.* **2019**, *8*, 816–834.
[4] Y. Che, Z. Han, B. Luo, D. Xia, J. Shi, Z. Gao, J. Wang, *Int. J. Electrochem. Sci.* **2012**, *7*, 999–1007.
[5] J. Rawat, M. A. Quraishi, *Bull. Electrochem.* **2003**, *19*, 467–470.
[6] S. A. Sayed, H. H. Hamdy, F. M. Noble, *Corros. Sci.* **2004**, *46*, 1071–1082.
[7] B. El Ibrahimi, K. El Mouaden, A. Jmiai, A. Baddouh, S. El Issami, L. Bazzi, M. Hilali, *Surfaces and Interfaces* **2019**, *17*, 100343.
[8] N. F. El Boraei, S. S. Abd El Rehim, *Mater. Chem. Phys.* **2018**, *215*, 332–338.
[9] M. Abdallah, B. H. Asghar, I. Zaafarany, A. S. Fouda, *Int. J. Electrochem. Sci.* **2012**, *7*, 282–304.
[10] L. Yohai, W. Schreiner, M. Vázquez, M. B. Valcarce, *Electrochim. Acta* **2016**, *202*, 231–242.
[11] H. Nahali, L. Dhouibi, H. Idrissi, *Constr. Build. Mater.* **2014**, *50*, 87–94.
[12] J. J. Shi, W. Sun, *Cement. Concrete. Comp.* **2014**, *45*, 166–175.
[13] N. Etteyeb, L. Dhouibi, H. Takenouti, M. C. Alonso, E. Triki, *Electrochim. Acta* **2007**, *52*, 7506–7512.
[14] M. Reffass, R. Sabot, M. Jeannin, C. Berziou, P. Refait, *Electrochim. Acta* **2009**, *54*, 4389–4396.
[15] L. Yohai, M. Vázquez, M. B. Valcarce, *Electrochim. Acta* **2013**, *102*, 88–96.
[16] H. Bensabra, A. Franczak, O. Aaboubi, *Metall. Mater. Trans. A* **2017**, *48*, 412–424.
[17] Y. Ait Albrimi, A. Ait Addi, J. Douch, R. M. Souto, M. Hamdani, *Corros. Sci.* **2015**, *90*, 522–528.
[18] A. Ait Addi, E. Ait Addi, I. Bakas, M. Hamdani, *Int. J. Electrochem. Sci.* **2014**, *9*, 8465–8475.
[19] K. Sayin, D. Karakas, *Corros. Sci.* **2013**, *77*, 37–45.
[20] M. J. Frisch, G. W. Trucks, H. B. Schlegel, G. E. Scuseria, M. A. Robb, J. R. Cheeseman, G. Scalmani, V. Barone, B. Mennucci, G. A. Petersson, H. Nakatsuji, M. Caricato, X. Li, H. P. Hratchian, A. F. Izmaylov, J. Bloino, G. Zheng, J. L. Sonnenberg, M. Hada, M. Ehara, K. Toyota, R. Fukuda, J. Hasegawa, M. Ishida, T. Nakajima, Y. Honda, O. Kitao, H. Nakai, T. Vreven, J. A. Montgomery, Jr., J. E. Peralta, F. Ogliaro, M. Bearpark, J. J. Heyd, E. Brothers, K. N. Kudin, V. N. Staroverov, R. Kobayashi, J. Normand, K. Raghavachari, A. Rendell, J. C. Burant, S. S. Iyengar, J. Tomasi, M. Cossi, N. Rega, J. M. Millam, M. Klene, J. E. Knox, J. B. Cross, V. Bakken, C. Adamo, J. Jaramillo, R. Gomperts, R. E. Stratmann, O. Yazyev, A. J. Austin, R. Cammi, C. Pomelli, J. W. Ochterski, R. L. Martin, K. Morokuma, V. G. Zakrzewski, G. A. Voth, P. Salvador, J. J. Dannenberg, S. Dapprich, A. D. Daniels, O. Farkas, J. B. Foresman, J. V.

Ortiz, J. Cioslowski, D. J. Fox, *Gaussian, Inc.*, Wallingford CT, **2009**.
[21] A. J. Lopes-Jesus, L. I. N. Tomé, M. Ermelinda, S. Eusébio, M. T. S. Rosado, J. S. Redinha, *J. Phys. Chem. A* **2007**, *111*, 3432–3437.
[22] B. El Ibrahimi, A. Jmiai, K. El Mouaden, R. Oukhrib, A. Soumoue, S. El Issami, L. Bazzi, *J. King Saud Univ. Sci.* **2020**, *32*, 163–171.
[23] B. El Ibrahimi, K. El Mouaden, A. Jmiai, A. Baddouh, S. El Issami, L. Bazzi, M. Hilali, *Surf. Interfaces* **2019**, *17*, 100343.
[24] B. El Ibrahimi, A. Jmiai, K. El Mouaden, A. Baddouh, S. El Issami, L. Bazzi, M. Hilali, *J. Mol. Struct.* **2019**, *1196*, 105–118.
[25] A. da Silva, E. D'Elia, J. da Cunha Ponciano Gomes, *Corros. Sci.* **2010**, *52*, 788.
[26] T. Pajkossy, *J. Electroanal. Chem.* **1994**, *364 (1–2)*, 111–125.
[27] K. M. Ismail, W. A. Badawy, *J. Appl. Electrochem.* **2000**, *30*, 1303–1311.
[28] S. Gudić, I. Smoljko, M. Kliškić, *J. Alloys Compd.* **2010**, *505*, 54–63.
[29] R. M. El-Sherif, W. A. Badawy, *Int. J. Electrochem. Sci.* **2011**, *6*, 6469–6482.
[30] I. Carrillo, B. Valdez, R. Zlatev, M. Stoytcheva, M. Carrillo, R. Bäßler, *Int. J. Electrochem. Sci.* **2012**, *7 (9)*, 8688–8701.
[31] S. A. M. Refaey, S. S. Abd El-Rehim, F. Taha, M. B. Saleh, R. A. Ahmed, *Appl. Surf. Sci.* **2000**, *158*, 190–196.
[32] M. Behpour, S. M. Ghoreishi, N. Soltani, M. Salavati-Niasari, M. Hamadanian, A. Gandomi, *Corros. Sci.* **2008**, *50*, 2172–2181.
[33] D. Zhou, J. Wang, Y. Gao, L. Zhang, *Int. J. Electrochem. Sci.* **2017**, *1 (12)*, 192–205.
[34] S. C. Nwanonenyi, H. C. Obasi, I. C. Chukwujike, M. A. Chidiebere, E. E. Oguzie, *Chemistry Africa* **2019**, *2*, 277–289.
[35] A. I. Onuchukwu, A. I. Baba, *Mater. Chem. Phys.* **1987**, *18 (4)*, 381–390.
[36] R. Solmaz, G. Kardas, B. Yazici, M. Erbil, *Colloids Surf. A* **2008**, *312*, 7.
[37] K. Ramya, K. K. Anupama, K. M. Shainy, A. Joseph, *Egypt. J. Pet.* **2017**, *26 (2)*, 421–437.
[38] R. Solmaz, *Corros. Sci.* **2014**, *81*, 4.
[39] G. Gece, *Corros. Sci.* **2008**, *50*, 2981–2992.
[40] K. Fukui, *Angew. Chem. Int. Ed. Engl.* **1989**, *21*, 801–809.
[41] D. Q. Huong, T. Duong, P. C. Nam, *ACS Omega* **2019**, *4*, 14478–14489.
[42] B. El Ibrahimi, A. Soumoue, A. Jmiai, H. Bourzi, R. Oukhrib, K. El Mouaden, S. El Issami, L. Bazzi, *J. Mol. Struct.* **2016**, *1125*, 93–102.
[43] D. K. Singh, E. E. Ebenso, M. K. Singh, D. Behera, G. Udayabhanu, R. P. John, *J. Mol. Liq.* **2018**, *250*, 88–99.
[44] H. Zhao, X. Zhang, L. Ji, H. Hu, Q. Li, *Corros. Sci.* **2014**, *83*, 261–271.
[45] H. H. Zhang, Y. Chena, Z. Zhang, *Results Phys.* **2018**, *11*, 554–563.
[46] M. Yadav, D. Behera, S. Kumar, R. R. Sinha, *Ind. Eng. Chem. Res.* **2013**, *52*, 6318–6328.
[47] B. EL Ibrahimi, L. Bazzi, S. EL Issam, *RSC Adv.* **2020**, *10*, 29696–29704.
[48] H. Bourzi, R. Oukhrib, B. El Ibrahimi, H. Abou Oualid, Y. Abdellaoui, B. Balkard, S. El Issami, M. Hilali, L. Bazzi, C. Len, *Sustainability* **2020**, *12*, 3304, 1–14.
[49] A. Kokalj, *Chem. Phys.* **2012**, *393*, 1–12.
[50] N. Kovačević, A. Kokalj, *Corros. Sci.* **2011**, *53*, 909–921.
[51] A. Kokalj, *Electrochim. Acta* **2010** *56*, 745–755.
[52] H. Lgaz, R. Salghi, S. Bhat, A. Chaouiki, Shubhalaxmi, S. Jodeh, *J. Mol. Liq.* **2017**, *244*, 154–168.
[53] M. K. Awad, M. S. Metwally, S. A. Soliman, A. A. El-Zomrawy, M. A. bedair, *J. Ind. Eng. Chem.* **2014**, *20*, 796–808.
[54] M. K. Awad, M. R. Mustafa, M. M. A. Elnga, *J. Mol. Struct.* **2010**, *959*, 66–74.

Received: November 28, 2020
Accepted: December 31, 2020
Published online on ■■, ■■

FULL PAPER

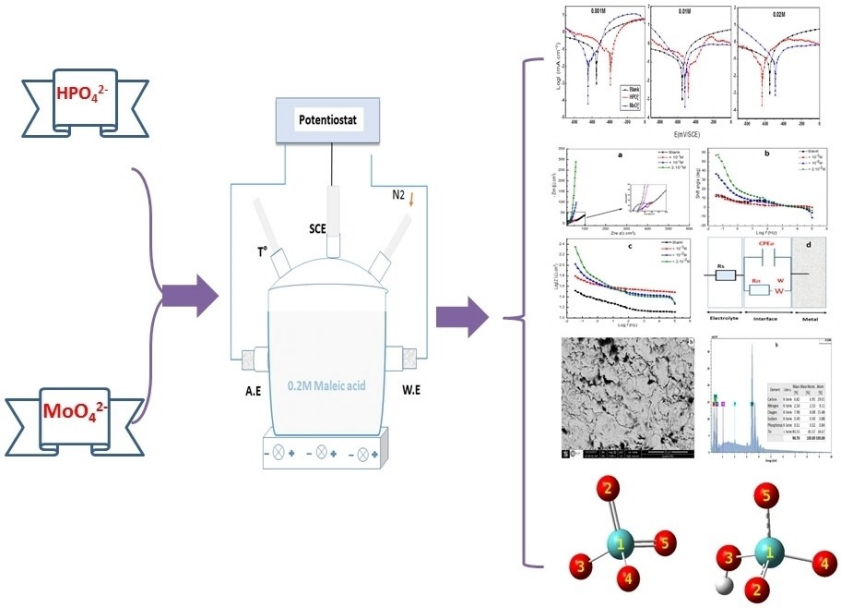

Dr. B. Ait Addi, Prof. B. El Ibrahimi, Prof. A. Ait Addi, Dr. A. Shaban, Prof. E.-H. Ait Addi, Prof. M. Hamdani*